Temporal Assessment of Methane Emissions in Relation to Land Use and Land Cover Dynamics Using Satellite Data in the Lakes District of Türkiye (2019–2024)

Gül Nur Karal Nesil*[1], Nebiye Musaoğlu[1]

[1] Faculty of Civil Engineering, Department of Geomatics Engineering, Istanbul Technical University (ITU), 34469 Maslak, Istanbul, Türkiye (karalg, musaoglune)@itu.edu.tr

Keywords: Methane Emission, Lakes District, LULC, Satellite Data, Sentinel 5P

Abstract

Land use and land cover (LULC) changes have an important effect on the dynamics of climate change, affecting the structure and functioning of ecosystems. Greenhouse gases in the atmosphere are directly related to the functioning of the climate system, and methane (CH_4) gas, in particular, stands out as one of the primary greenhouse gases due to its high global warming potential. In this context, systematically examining the effects of LULC changes on CH_4 emissions is fundamental to understanding regional and global climate change processes. In this context, this study determined the relationships between LULC changes and CH_4 emissions in the Lakes District of Türkiye. CH_4 emissions obtained from Sentinel 5P satellite data were correlated with classes obtained from the Sentinel 2 LULC dataset. The Pearson correlation analysis conducted to examine the relationship between LULC changes and CH_4 emissions yielded correlation values of -0.90 for water areas, -0.98 for forest areas, +0.98 for built-up areas, and +0.12 for agricultural areas. These results suggest that the decline in forest and water areas, as well as the expansion of built-up areas, is linked to the increase in CH_4 emissions. Although no significant change was observed in agricultural and pasture areas, the continuous increase in CH_4 emissions indicates the impact of agricultural and livestock activities on emissions. Additionally, a trend analysis was conducted to assess the temporal variation in CH_4 emissions. The Mann-Kendall test showed a statistically significant upward trend ($p < 0.01$) in CH_4 emissions during the 2019–2024 period. The Kendall's Tau value obtained was 0.53, reflecting a moderate positive relationship. However, it was determined that emissions peaked annually during the summer and autumn months (July–September) and remained relatively low during the spring and winter months (March–May and December–February). This demonstrates that temperature increases have an enhancing effect on CH_4 emissions.

1. Introduction

Land use and land cover (LULC) changes play a significant role in climate change. These changes impact the structure and functioning of ecosystems, from the distribution of vegetation to water resources, resulting in significant alterations to the natural balance and ecological processes. One of the most striking consequences of these processes is the changes in atmospheric greenhouse gas dynamics. Methane (CH_4) is one of the primary greenhouse gases contributing to global warming, stemming from both natural and anthropogenic sources, and has a significant impact on the climate. It is recognized as a short-lived but highly effective greenhouse gas, exhibiting a markedly higher global warming potential than carbon dioxide (CO_2) on a 20 year period (Masson-Delmotte et al., 2021). The identification and monitoring of emissions are critical for understanding the climate change impacts of CH_4 and developing sustainable management strategies. Several factors influence CH_4 emissions; changes in LULC are one of the factors affecting CH_4 emissions (Lage Filho et al., 2023). Different LULC classes have varying impacts on CH_4 emissions (Malerba et al., 2022; Scoones, 2023; Jodhani et al., 2024). In this context, examining the effects of LULC changes on CH_4 emissions plays an essential role in understanding regional carbon cycles and climate change trends.

Today, satellite-based remote sensing data is a reliable and effective source of information for determining and monitoring greenhouse gas emissions and LULC changes. The Sentinel 5P satellite stands out in measuring CH_4 emissions. The Tropospheric Monitoring Instrument (TROPOMI) on the Sentinel 5P satellite, provided by the European Space Agency (ESA), measures column-averaged CH_4 on a daily basis (Liu et al., 2021; Lorente et al., 2023). CH_4 emissions are obtained from shortwave infrared (SWIR) and near-infrared (NIR) Measurements (Sha et al., 2021). Thanks to its daily and wide-area coverage capacity, temporal variations and spatial distributions of CH_4 emissions can be analyzed. With these features, Sentinel 5P has become one of the most widely used satellite systems for atmospheric CH_4 monitoring today. For example, Lindqvist et al. (2024) assessed CH_4 emissions in northern high latitudes using Sentinel 5P data, demonstrating that these data enable the analysis of seasonal variations. Another study used Sentinel 5P to assess long-term and seasonal changes in atmospheric CH_4 emissions in regions where rice is produced (Kozicka et al., 2023).

Satellite data is widely used as a primary data source for determining and monitoring LULC classes. For example, LULC classes can be obtained using various classification methods and indices from free medium spatial resolution satellite data, such as Sentinel 2 and Landsat 8 (Acharki, 2022; Nasiri et al., 2022; Nguyen et al., 2020). Sentinel 2 data, in particular, contributes significantly to monitoring LULC, and today, various LULC datasets derived from Sentinel 2 are available (Phiri et al., 2020). These datasets provide direct information about LULC. They enable the analysis of LULC changes across different time periods and large geographic areas, thereby playing a crucial role in assessing the impacts of environmental processes, ecosystem dynamics, and human activities. The ESRI Land Cover dataset, one of the most widely used datasets, provides data covering the period 2019-2024 and stands out as an important tool for monitoring LULC changes (Esri | Sentinel-2 Land Cover Explorer).

One of the most significant natural sources of CH_4 is aquatic ecosystems (Rosentreter et al., 2021; Saunois et al., 2020). Water bodies stand out as areas where CH_4 emissions are concentrated due to natural processes and environmental conditions. In addition to natural sources, human activities also contribute significantly to CH_4 emissions. In this context, Türkiye's Lakes District, which is exposed to both natural and human pressures and hosts inland water ecosystems, stands out as a critical area for monitoring CH_4 emissions. This study analyzes the impact of LULC changes in the Lakes District on CH_4 emissions between 2019 and 2024. CH_4 emissions obtained from Sentinel 5P TROPOMI satellite data were associated with classes such as water, forestry, agricultural area, rangeland, barrenland and built-up area obtained from the Sentinel 2 ESRI Land Cover dataset. Changes in LULC and emissions were analyzed. Pearson correlation analysis was performed to examine the relationship between class changes and emissions. Furthermore, the Mann-Kendall test was performed to evaluate the temporal changes in emissions and determine their trend.

2. Data and Methodology

2.1 Study Area

The study area is situated in western and southwestern Anatolia, commonly referred to as the Lakes District of Türkiye, and is surrounded by numerous lakes. This region includes lake basins and the surrounding plains, as well as agricultural area and rangelands. This region, which contains 16 lakes (Acıgöl, Akgöl, Akşehir, Beyşehir, Burdur, Eber, Eğirdir, Gavur, Ilgın (Çavuşçu), Işıklı, Karamık, Karataş, Kovada, Salda, Suğla and Yarışlı), spans an area of approximately 17,000 km². The lakes, with varying characteristics, have formed as a result of the accumulation of salty, bitter, and fresh water in depressions created by tectonic and volcanic movements in the region (Lakes District - Wikipedia). Figure 1 illustrates the study area.

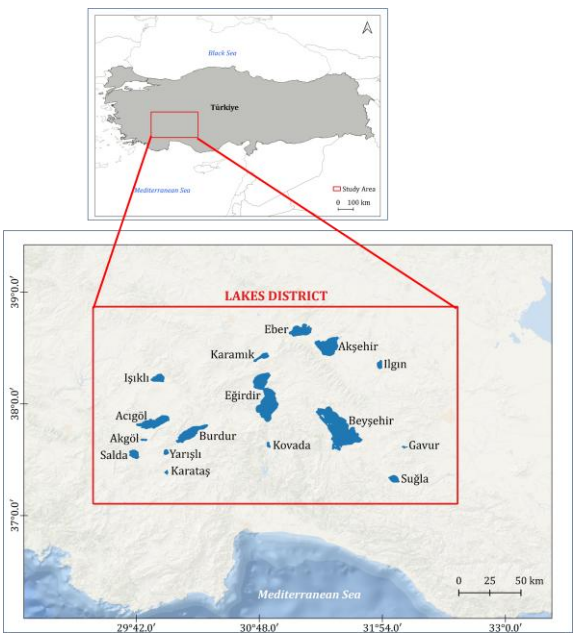

Figure 1. The upper map shows the geographical location of Türkiye, while the main map illustrates the borders and lakes within Türkiye's Lakes District.

2.2 Data Used and Methodology

Within the scope of this study, CH_4 emissions were obtained from Sentinel 5P satellite data, while LULC classes were obtained from the ESRI Land Cover dataset. The TROPOMI on the Sentinel 5P satellite is an imaging spectrometer that measures sunlight reflected by the Earth. It collects data covering an area of 2600 km and presents this data at a spatial resolution of 5.5 x 3.5 km². This allows for a detailed examination of the different components in the atmosphere, covering the entire world (Copernicus, 2019; Schneising et al., 2019). The Google Earth Engine (GEE) Platform was used to obtain CH_4 emissions from Sentinel 5P. Level 2 (L2) data acquired from the Sentinel 5P satellite is processed to Level 3 (L3) using GEE. In this study, analyses were performed using OFFL (offline) L3 data, which is sufficiently up-to-date and of high data quality for the analysis of CH_4 emissions. LULC data was downloaded from the ESRI Living Atlas website (https://livingatlas.arcgis.com/landcoverexplorer/) (Esri | Sentinel-2 Land Cover Explorer). Subsequently, LULC and CH_4 emission maps were created in GEE and QGIS environments. The workflow diagram for the study is presented in Figure 2.

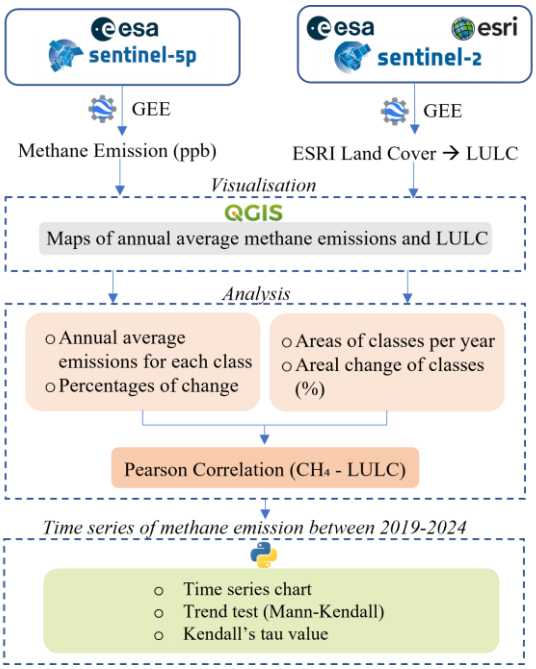

Figure 2. Flow chart of the study.

CH_4 emissions for the years 2019–2022–2024 were analyzed using the "CH4_column_volume_mixing_ratio_dry_air" band from the Sentinel 5P satellite. The data were processed in the GEE environment, and annual CH_4 emission distributions were obtained by taking separate averages for each year. The visualization of the created maps was performed in the QGIS program. The class to which the annual average emission values corresponded was determined in QGIS using the Zonal Statistics tool. The relationship between emissions and LULC was determined using Pearson correlation. Similar to the study by Jodhani et al. (2024) positive values indicate an increase in the relevant LULC and a simultaneous increase in emissions. Negative values, on the other hand, indicate that emissions increase with a decrease in land use, i.e., an inverse relationship. The correlation coefficient formula is shown in Equation 1 (Pearson, 1896).

$$r = n\sum xy - \sum x \sum y / \sqrt{(n\sum x^2 - (\sum x)^2)(n\sum y^2 - (\sum y)^2)} \quad (1)$$

r: Pearson correlation coefficient x, y: Values in the data sets, n: Number of observations.

In addition, monthly average CH_4 values were calculated. A time series graph for the period 2019-2024 was created based on the monthly averages obtained. Sen's Slope Analysis (Sen, 1968) was applied to evaluate the trend of emissions over time in this graph, and the Mann-Kendall (MK) test was applied to test the trend (Kendall, 1957; Mann, 1945). The median slope in Sen's Slope analysis is calculated as follows (Equation 2):

$$\text{Sen's slope} = \text{Median}\ \frac{Xj - Xk}{j - k},\quad j > k \quad (2)$$

X_j and X_k are observations in the time series. Sen's slope value is calculated as the median of the slopes. This median slope indicates the general trend of the series; if positive, it indicates an increasing trend, and if negative, a decreasing trend.

The MK test is a trend test method frequently used in the literature. Each value is compared with all subsequent data, i.e., with the sequential data sample. The MK statistic (Z_{MK}) for the time series x(t) (t = 1, …, n) is calculated as follows (Equations 3,4):

$$Z_{MK} = \begin{cases} \frac{S-1}{\sqrt{Var(S)}}, & if\ S > 0; \\ 0, \text{ if } S = 0; \\ \frac{S+1}{\sqrt{Var(S)}}, & \text{if } S < 0 \end{cases} \quad (3)$$

Where:

$$\text{Var}(S) = \frac{1}{18}\left[n(n-1)(2n+5) - \sum_{t=1}^{m} t1\,(t1-1)(2t1+5) \right] \quad (4)$$

The S trend test statistic, Var(S) represents the variance of S, n represents the length of the time series, and m represents the number of repeated values (Hamed, 2009; Hamed & Ramachandra Rao, 1998). If the data in the time series are independent, the trend in the time series is significant; Z_{MK} is greater than $Z_{1-\alpha/2}$ ($p<0.01$). In the opposite case, the trend is not significant.

Kendall's tau value is a nonparametric method that measures the relationship between the probabilities of concordant and discordant outcomes for two observed variables, X and Y, and is calculated using Equation 5 (Kendall, 1938) .

$$\text{Tau} = \frac{2(C-D)}{n(n-1)} \quad (5)$$

Here, C indicates compatible combinations, whereas D indicates incompatible ones. Kendall's tau value ranges from -1 to +1. The time series graphs were created in the Python environment, and the statistical tests were also performed in this environment. The creation of the time series graphs and the execution of the related statistical tests were carried out using the Python programming language.

3. Results and Conclusions

Maps of LULC classes derived from the Land Cover dataset are presented in Figure 3.

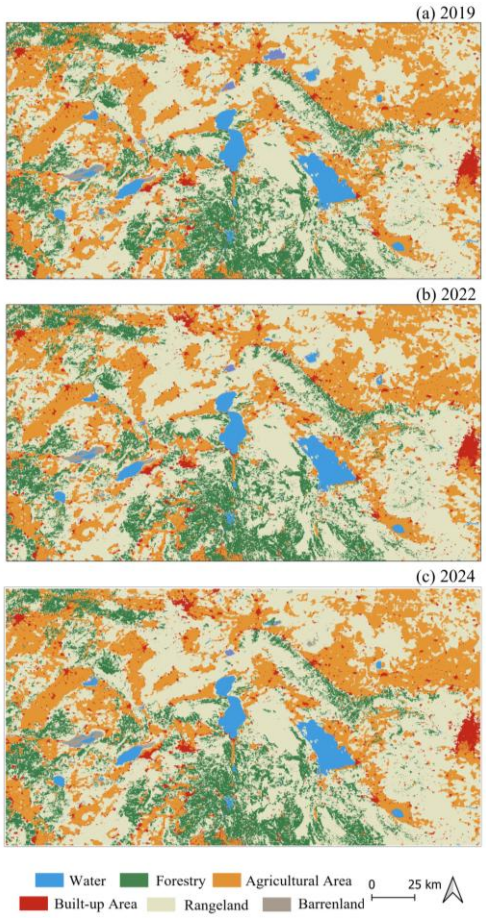

Figure 3. Temporal LULC classes from ESRI Land cover dataset (a)2019, (b)2022, (c)2024

No significant change has been observed in agricultural and rangeland on the maps, while an increase has been observed in built-up areas for 2019-2024 period. For a more detailed analysis, the areas and changes in the classes are presented in Tables 1 and 2.

Classes	Area (km²)		
	2019	2022	2024
Water	161.4	154.1	145.5
Forestry	8558.3	8301.3	8295.1
Agricultural	1520.1	1490.6	1530.5
Built-up	1874.6	2046.9	2203.0
Barrenland	38.5	32.1	31.7
Rangeland	28174.4	28302.3	28121.5

Table 1. Area (km²) of each LULC class in 2019, 2022, and 2024.

Classes	Areal Change of Classes (%)		
	2019-2022	2022-2024	2019-2024
Water	−4.52%	−5.58%	−9.85%
Forestry	−3.0%	-0.07%	−3.07%
Agricultural	−1.94%	2.67%	0.68%
Built-up	9.19%	7.63%	17.52%
Barrenland	−16.62%	−1.25%	−17.66%
Rangeland	0.45%	-0.64%	−0.19%

Table 2. Areal change (%) of LULC classes between 2019–2022, 2022–2024, and 2019–2024.

Throughout the 2019–2024 period, a decrease was observed in water, forestry, and barrenland classes, a significant increase in built-up areas, and limited change in agricultural and rangeland areas. The continuous decline in water surfaces reflects the receding of lakes or water sources and the effects of drought. The significant and continuous increase in built-up areas is an important indicator of urbanization and population pressure in the region. The decrease in the barrenland class is considered to be the conversion of these areas to built-up, agricultural, or natural cover (forestry, rangeland) classes. These results show that urbanization and human-induced pressures have a significant impact on the ecosystem. Specifically, these findings demonstrate that natural areas are being converted into built-up areas, accompanied by a reduction in water resources and a decline in forestry areas.

Annual average CH_4 emission maps are presented in Figure 4.

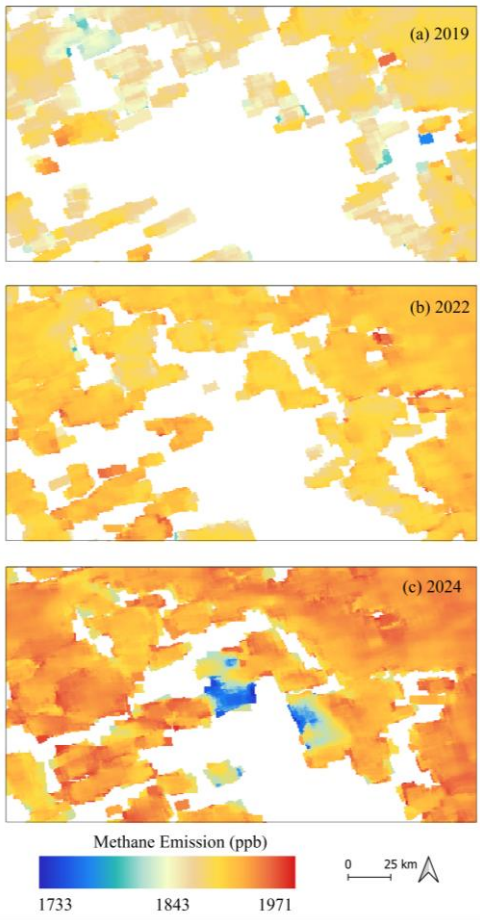

Figure 4. CH_4 emission maps (a):2019, (b):2022, (c):2024

The three-line map series (a: 2019, b: 2022, c: 2024) shows the temporal change in CH_4 emissions in the region. The maps represent emissions ranging from 1733 to 1971 ppb (parts per billion) using a color scale, with white areas indicating locations where no emission data are available. The 2019 map (a) shows generally low to moderate CH_4 emissions. However, by 2022 (b), a general increase in emission intensity is noticeable. Emissions have spatially expanded, particularly in the northern and eastern parts. Emissions have increased further in the 2024 map (c). Areas with high emission levels have increased. While the highest emission in 2019 was determined to be 1924 ppb, it reached 1951 ppb in 2022 and 1971 ppb in 2024. It is observed that average emissions in the region increased significantly between 2019 and 2024, and that this increase spread regularly both temporally and spatially. This situation is considered to be the effects of LULC changes and climatic factors in the region on emissions.

Within this scope, emissions for each class were determined and their changes over time were analyzed (Table 3, Table 4).

Classes	CH_4 Emission (ppb)		
	2019	2022	2024
Water	1865	1889	1893
Forestry	1862	1889	1897
Agricultural	1873	1896	1910
Built-up	1867	1893	1904
Barrenland	1873	1900	1912
Rangeland	1872	1895	1907

Table 3. CH_4 emission values (ppb) of different land cover classes for the years 2019, 2022, and 2024.

When the highest emissions over three years are evaluated, agricultural areas, built-up areas, rangeland, and barrenland stand out.

Classes	CH_4 Emission Change (%)		
	2019-2022	2022-2024	2019-2024
Water	1.29%	0.21%	1.50%
Forestry	1.45%	0.42%	1.88%
Agricultural	1.23%	0.74%	1.98%
Built-up	1.39%	0.58%	1.98%
Barrenland	1.44%	0.63%	2.08%
Rangeland	1.23%	0.63%	1.87%

Table 4. Percentage changes in CH_4 emissions for different LULC classes between 2019 and 2024.

When examining the changes in Table 4, it is observed that emissions increased in all classes during the 2019–2024 period. Between 2019 and 2022, the increase in emissions across all classes is between 1% and 1.5%. Although the rate of increase remained below 1% in the 2022–2024 period, the total change in emissions over 2019–2024 exceeded 1.5%. Therefore, it is crucial to determine the relationship between changes in land area and changes in emissions. This is because differences in LULC can affect natural and anthropogenic CH_4 emissions. In particular, changes in land area in classes with high emission potential, such as water, agricultural, and built-up areas, play a critical role in understanding overall emission dynamics. The correlation coefficients calculated in this context are presented in Table 5.

Classes	Correlation Coefficient
Water	−0.90
Forestry	−0.98
Agricultural	0.12
Built-up	0.98
Barrenland	−0.97
Rangeland	−0.09

Table 5. Correlation coefficients between area changes in different LULC classes and CH_4 emissions

According to the Table 5, strong negative correlations are observed in the water, forestry, and barrenland classes. This indicates that CH_4 emissions tend to increase as the areas of these classes decrease. The negative relationship between the decrease in water area and the increase in CH_4 results from shared environmental stresses—particularly drought and rising temperatures—that simultaneously drive lake shrinkage and enhance CH_4 production through different processes. In the built-up areas, however, a very strong positive correlation is found, showing that CH_4 emissions increase in parallel with the increase in area. For agricultural areas and rangelands, the correlations are weak, and there is no apparent relationship between changes in area and emissions. Nevertheless, the fact that emissions from agricultural and rangeland areas are higher than those from other classes indicates that these areas play a significant role in CH_4 emissions, even if there is no substantial spatial change in these areas. This is because agricultural and rangelands contribute to emissions due to pollution from fertilizer use and livestock activities. Expansion in built-up areas increases emissions due to various factors, including industrial growth, deforestation, domestic and industrial waste, landfills, and vehicle pollution.

A time series graph was created to examine the temporal change in emissions from 2019 to 2024, identifying the trend of the graph and the months in which emissions were higher (Figure 5).

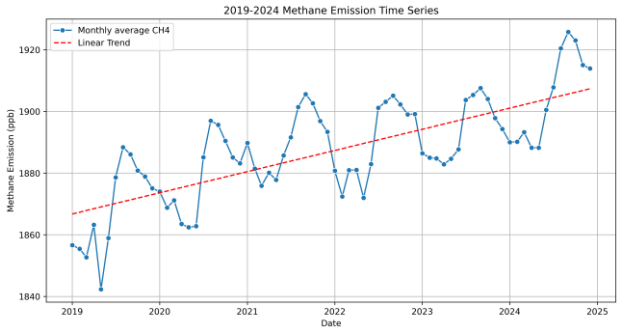

Figure 5. CH_4 emissions time series graph (2019-2024). The graph displays the monthly average CH4 emissions, illustrating both seasonal variability and a linear trend that indicates an overall increase over the 5 years.

Emissions started below 1870 ppb in early 2019, but by 2025 they had risen above 1910 ppb. The slope of the graph (Sen's Slope) is 0.57, indicating an increasing trend. The MK test results, which determine whether the trend is statistically significant, showed a P-value of less than 0.01 (4.95×10^{-11}). This also indicates that the upward trend is statistically highly significant. Kendall's Tau value was calculated as 0.53, indicating a moderate-to-high positive correlation. This shows that CH_4 emissions have shown a consistent and pronounced upward trend over time. This increasing trend highlights that rising greenhouse gas levels remain a persistent problem.

The emissions examined are observed to decrease towards the beginning and end of the year (winter and spring/March–May and December–February) and peak during the summer months and early autumn (July–September). It is noted that emissions increase with rising temperatures and remain lower during the winter months. While the average rises, the peak points in subsequent years of the series become noticeably higher. Emissions reach their highest recorded values at the end of 2024/beginning of 2025, exceeding approximately 1920 ppb. This represents a significant jump compared to the peaks of other years. This is interpreted as either an acceleration in the rate of increase or a more extreme seasonal peak. While atmospheric CH_4 naturally fluctuates from year to year, the underlying long-term trend is upward, necessitating the monitoring and reduction of CH_4 emissions.

The results obtained indicate that human activities significantly influence emissions in the region. The increasing emission trend suggests that the environmental impacts of LULC change are becoming apparent in the long term. In particular, the combined effects of built-up expansion, agricultural and livestock activities, and temperature increases account for a significant share of emissions. This situation shows that both natural processes and human activities play an important role in the formation of these emissions and are essential for understanding the dynamics of climate change, and it also suggests that land management and climate policies must be addressed together in future studies on this subject. The temporal increase in CH_4 emissions emphasizes the need to prioritize monitoring and mitigation efforts in the fight against climate change at the regional scale. The results suggest that integrating satellite-based observations into local environmental planning processes can significantly contribute to decision-making. However, the data gap in satellite-based observations remains a significant problem; therefore, it is recommended that future studies focus on addressing these data gaps and increasing the comprehensiveness of satellite observations.

References

Acharki, S., 2022. PlanetScope contributions compared to Sentinel-2, and Landsat-8 for LULC mapping. *Remote Sensing Applications: Society and Environment*, *27*, 100774. https://doi.org/10.1016/J.RSASE.2022.100774

Copernicus., 2019. *Sentinel-5 Precursor Mission Status C. Zehner-Sentinel 5 Precursor Mission Manager-ESA*. Retrieved Jan 12, 2026, from https://share.google/2uU2d4iO5eXVAn43u

Esri | Sentinel-2 Land Cover Explorer. Retrieved May 14, 2025, from https://livingatlas.arcgis.com/landcoverexplorer/#mapCenter=28.71471%2C42.45767%2C6.65741130826159&mode=step&timeExtent=2017%2C2024&year=2024

Hamed, K. H., 2009. Exact distribution of the Mann–Kendall trend test statistic for persistent data. *Journal of Hydrology*, *365*(1–2), 86–94. https://doi.org/10.1016/J.JHYDROL.2008.11.024

Hamed, K. H., & Ramachandra Rao, A., 1998. A modified Mann-Kendall trend test for autocorrelated data. *Journal of Hydrology*, *204*(1–4), 182–196. https://doi.org/10.1016/S0022-1694(97)00125-X

Jodhani, K. H., Gupta, N., Parmar, A. D., Bhavsar, J. D., Patel, H., Patel, D., Singh, S. K., Mishra, U., & Omar, P. jee., 2024. Synergizing google earth engine and earth observations for potential impact of land use/ land cover on air quality. *Results in Engineering*, *22*, 102039. https://doi.org/10.1016/J.RINENG.2024.102039

Kendall, M. G., 1938. A NEW MEASURE OF RANK CORRELATION. *Biometrika*, *30*(1–2), 81–93. https://doi.org/10.1093/BIOMET/30.1-2.81

Kendall, M. G., 1957. Rank Correlation Methods. *Biometrika*, *44*(1/2), 298. https://doi.org/10.2307/2333282

Kozicka, K., Orazalina, Z., Gozdowski, D., & Wójcik-Gront, E., 2023. Evaluation of temporal changes in methane content in the atmosphere for areas with a very high rice concentration based on Sentinel-5P data. *Remote Sensing Applications: Society and Environment*, *30*, 100972. https://doi.org/10.1016/J.RSASE.2023.100972

Lage Filho, N. M., Cardoso, A. da S., Azevedo, J. C. de, Macedo, V. H. M., Domingues, F. N., Faturi, C., Silva, T. C. da, Ruggieri, A. C., Reis, R. A., & do Rêgo, A. C., 2023. How does land use change affect the methane emission of soil in the Eastern Amazon? *Frontiers in Environmental Science*, *11*, 1244152. https://doi.org/10.3389/FENVS.2023.1244152/BIBTEX

Lakes District - Wikipedia. Retrieved October 1, 2025, from https://tr.wikipedia.org/wiki/G%C3%B6ller_Y%C3%B6resi

Lindqvist, H., Kivimäki, E., Häkkilä, T., Tsuruta, A., Schneising, O., Buchwitz, M., Lorente, A., Martinez Velarte, M., Borsdorff, T., Alberti, C., Backman, L., Buschmann, M., Chen, H., Dubravica, D., Hase, F., Heikkinen, P., Karppinen, T., Kivi, R., McGee, E., … Tamminen, J., 2024. Evaluation of Sentinel-5P TROPOMI Methane Observations at Northern High Latitudes. *Remote Sensing 2024, Vol. 16, Page 2979*, *16*(16), 2979. https://doi.org/10.3390/RS16162979

Liu, M., van der A, R., van Weele, M., Eskes, H., Lu, X., Veefkind, P., de Laat, J., Kong, H., Wang, J., Sun, J., Ding, J., Zhao, Y., & Weng, H., 2021. A New Divergence Method to Quantify Methane Emissions Using Observations of Sentinel-5P TROPOMI. *Geophysical Research Letters*, *48*(18), e2021GL094151. https://doi.org/10.1029/2021GL094151

Lorente, A., Borsdorff, T., Martinez-Velarte, M. C., & Landgraf, J., 2023. Accounting for surface reflectance spectral features in TROPOMI methane retrievals. *Atmospheric Measurement Techniques*, *16*(6), 1597–1608. https://doi.org/10.5194/AMT-16-1597-2023

Malerba, M. E., de Kluyver, T., Wright, N., Schuster, L., & Macreadie, P. I., 2022. Methane emissions from agricultural ponds are underestimated in national greenhouse gas inventories. *Communications Earth and Environment*, *3*(1), 1–7. https://doi.org/10.1038/S43247-022-00638-9

Mann, H. B., 1945. Nonparametric Tests Against Trend. *Econometrica*, *13*(3), 245. https://doi.org/10.2307/1907187

Masson-Delmotte, V., Zhai, P., Chen, Y., Goldfarb, L., Gomis, M. I., Matthews, J. B. R., Berger, S., Huang, M., Yelekçi, O., Yu, R., Zhou, B., Lonnoy, E., Maycock, T. K., Waterfield, T., Leitzell, K., & Caud, N., 2021. Climate change 2021: the physical science basis. *Ipcc.ChV Masson-Delmotte, P Zhai, A Pirani, SL Connors, C Péan, S Berger, N Caud, Y ChenContribution of Working Group I to the Sixth Assessment Report of the …, 2021•ipcc.Ch*. https://doi.org/10.1017/9781009157896

Nasiri, V., Deljouei, A., Moradi, F., Sadeghi, S. M. M., & Borz, S. A., 2022. Land Use and Land Cover Mapping Using Sentinel-2, Landsat-8 Satellite Images, and Google Earth Engine: A Comparison of Two Composition Methods. *Remote Sensing 2022, Vol. 14, Page 1977*, *14*(9), 1977. https://doi.org/10.3390/RS14091977

Nguyen, H. T. T., Doan, T. M., Tomppo, E., & McRoberts, R. E., 2020. Land Use/Land Cover Mapping Using Multitemporal Sentinel-2 Imagery and Four Classification Methods—A Case Study from Dak Nong, Vietnam. *Remote Sensing 2020, Vol. 12, Page 1367*, *12*(9), 1367. https://doi.org/10.3390/RS12091367

Pearson, K., 1896. VII. Mathematical contributions to the theory of evolution.—III. Regression, heredity, and panmixia. *Philosophical Transactions of the Royal Society of London. Series A, Containing Papers of a Mathematical or Physical Character*, *187*, 253–318. https://doi.org/10.1098/RSTA.1896.0007

Phiri, D., Simwanda, M., Salekin, S., Nyirenda, V. R., Murayama, Y., & Ranagalage, M., 2020. Sentinel-2 Data for Land Cover/Use Mapping: A Review. *Remote Sensing 2020, Vol. 12, Page 2291*, *12*(14), 2291. https://doi.org/10.3390/RS12142291

Rosentreter, J. A., Borges, A. V., Deemer, B. R., Holgerson, M. A., Liu, S., Song, C., Melack, J., Raymond, P. A., Duarte, C. M., Allen, G. H., Olefeldt, D., Poulter, B., Battin, T. I., & Eyre, B. D., 2021. Half of global methane emissions come from highly variable aquatic ecosystem sources. *Nature Geoscience*, *14*(4), 225–230. https://doi.org/10.1038/S41561-021-00715-2

Saunois, M., R. Stavert, A., Poulter, B., Bousquet, P., G. Canadell, J., B. Jackson, R., A. Raymond, P., J. Dlugokencky, E., Houweling, S., K. Patra, P., Ciais, P., K. Arora, V., Bastviken, D., Bergamaschi, P., R. Blake, D., Brailsford, G., Bruhwiler, L., M. Carlson, K., Carrol, M., … Zhuang, Q., 2020. The global methane budget 2000-2017. *Earth System Science Data*, *12*(3), 1561–1623. https://doi.org/10.5194/ESSD-12-1561-2020

Schneising, O., Buchwitz, M., Reuter, M., Bovensmann, H., Burrows, J. P., Borsdorff, T., Deutscher, N. M., Feist, D. G., Griffith, D. W. T., Hase, F., Hermans, C., Iraci, L. T., Kivi, R., Landgraf, J., Morino, I., Notholt, J., Petri, C., Pollard, D. F., Roche, S., … Wunch, D., 2019. A scientific algorithm to simultaneously retrieve carbon monoxide and methane from TROPOMI onboard Sentinel-5 Precursor. *Atmospheric Measurement Techniques*, *12*(12), 6771–6802. https://doi.org/10.5194/AMT-12-6771-2019

Scoones, I., 2023. Livestock, methane, and climate change: The politics of global assessments. *Wiley Interdisciplinary Reviews: Climate Change*, *14*(1), e790. https://doi.org/10.1002/WCC.790

Sen, P. K., 1968. Estimates of the Regression Coefficient Based on Kendall's Tau. *Journal of the American Statistical Association*, *63*(324), 1379–1389. https://doi.org/10.1080/01621459.1968.10480934

Sha, M. K., Langerock, B., Blavier, J. F. L., Blumenstock, T., Borsdorff, T., Buschmann, M., Dehn, A., De Mazière, M., Deutscher, N. M., Feist, D. G., Garciá, O. E., Griffith, D. W. T., Grutter, M., Hannigan, J. W., Hase, F., Heikkinen, P., Hermans, C., Iraci, L. T., Jeseck, P., … Zhou, M., 2021. Validation of methane and carbon monoxide from Sentinel-5 Precursor using TCCON and NDACC-IRWG stations. *Atmospheric Measurement Techniques*, *14*(9), 6249–6304. https://doi.org/10.5194/AMT-14-6249-2021